

Binaries Among Debris Disk Stars

David R. Rodriguez^{1,2} and B. Zuckerman¹

ABSTRACT

We have gathered a sample of 112 main-sequence stars with known debris disks. We collected published information and performed adaptive optics observations at Lick Observatory to determine if these debris disks are associated with binary or multiple stars. We discovered a previously unknown M-star companion to HD 1051 at a projected separation of 628 AU. We found that $25 \pm 4\%$ of our debris disk systems are binary or triple star systems, substantially less than the expected $\sim 50\%$. The period distribution for these suggests a relative lack of systems with 1–100 AU separations. Only a few systems have blackbody disk radii comparable to the binary/triple separation. Together, these two characteristics suggest that binaries with intermediate separations of 1–100 AU readily clear out their disks. We find that the fractional disk luminosity, as a proxy for disk mass, is generally lower for multiple systems than for single stars at any given age. Hence, for a binary to possess a disk (or form planets) it must either be a very widely separated binary with disk particles orbiting a single star or it must be a small separation binary with a circumbinary disk.

Subject headings: binaries: general — infrared: stars — planetary systems: formation

1. Introduction

Planet formation occurs around young stars in disks that are rich in gas and dust, some of which can be used to form Jovian-class planets. This needs to occur fairly rapidly, since disk gas generally dissipates over a period of a few million years (Haisch et al. 2001; Uzpen et al. 2009). Eventually, even the dust in the system will be removed, either through accretion onto larger objects, stellar winds, or radiative processes. However, if the system

¹Dept. of Physics & Astronomy, University of California, Los Angeles 90095, USA

²Current address: Departamento de Astronomía, Universidad de Chile, Casilla 36-D, Santiago, Chile (drodrigu@das.uchile.cl)

has formed planetesimals or larger-sized objects, collisions can occur and produce a second generation of dust. These dusty systems, known as debris disks, could then contain detectable quantities of dust with little or no gas present and they would be older than their gas-rich counterparts (Zuckerman 2001; Wyatt 2008, and references therein). The first debris disks were found by the Infrared Astronomy Satellite (IRAS). IRAS surveyed almost the entire sky at 12, 25, 60, and $100\mu\text{m}$ and discovered infrared excesses around many stars including Vega, Fomalhaut, β Pictoris, and ϵ Eridani. The solar system’s own Kuiper Belt may be analogous to these circumstellar disks (e.g., Luu & Jewitt 2002, and references therein). A complete understanding of the formation and evolution of planetary systems requires knowledge of the properties of disks, from the gas-rich protoplanetary disks to the gas-poor debris disks.

Over 500 extrasolar planets have been discovered so far. Most extrasolar planet searches have utilized the precision radial velocity technique; however, the Kepler satellite has recently reported over 1200 candidate planets (see Borucki et al. 2011). While highly successful, the radial velocity technique is generally applied to single stars or very widely separated binaries. The problem is that the spectra of close binary stars are highly variable due to their orbital motion which typically leads to relatively large velocity uncertainties. However, the TATOOINE radial velocity survey (Konacki et al. 2009) is searching for planets around double-lined spectroscopic binaries and has reached precisions of a few m/s, comparable to, albeit not as good as, precisions reached for single stars. Although Konacki et al. (2009) have yet to report a circumbinary planet and their sample size is small (10 systems), their work demonstrates that future planet searches may be performed on close binaries.

Duquennoy & Mayor (1991) estimate that 57% of G stars may be in multiple systems. Other, more recent surveys show single stars are somewhat more common, but the fraction of multiples is still about $\sim 50\%$ (Eggleton & Tokovinin 2008; Raghavan et al. 2010). A question naturally arises: if so many stars are in multiple systems, what does this say about the formation and evolution of disks and planets? About 20% of known extra solar planets reside in wide separation binaries (Raghavan et al. 2006; Eggenberger et al. 2007), most of which have separations of 100s of AU. Eclipse timing variations of HW Virginis, CM Draconis, and NN Serpentis (a post-common envelope binary) suggest that planets may orbit these binaries (Deeg et al. 2008; Lee et al. 2009; Beuermann et al. 2010). Despite these efforts (see also Konacki et al. 2009), detection of planets in circumbinary orbits remains a challenge. While this manuscript was being prepared, Doyle et al. (2011) presented the discovery of Kepler-16b, the first circumbinary planet among the Kepler data. Both stars and the planet share a common orbital plane, suggesting the planet formed in a circumbinary disk. Indirect evidence implies the existence of rocky planets orbiting the close (3.4-day) main sequence binary BD +20 307. This system displays a large quantity of warm dust in the terrestrial planet zone (Song et al. 2005) that likely is the aftermath of a collision of two rocky planets

that orbit this ~ 1 Gyr old binary system (Zuckerman et al. 2008b; Weinberger et al. 2011). The study of circumstellar and circumbinary disks, then, can be used to comment on the process of planet formation around binary stars.

There has been some previous effort to address the issue of dusty disks in binary systems. Sub-millimeter studies of young ($\lesssim 5$ Myr) binaries have shown that binary stars with intermediate separations ($1 < a < 50 - 100$ AU) have lower sub-millimeter fluxes than more widely separated binaries or single stars (Jensen et al. 1996). Interferometric observations of nearby ~ 8 Myr-old disks in a triple and quadruple system have shown the disks to be truncated by the nearby stellar companions (Andrews et al. 2010), as expected from numerical simulations (Lubow & Artymowicz 2000; Artymowicz & Lubow 1994). Among pre-main sequence stars, several studies have found the disk lifetimes of small to moderate separation binaries to be shorter than that of single stars or very widely separated binaries (Bouwman et al. 2006; Cieza et al. 2009). Recently, Kraus et al. (2011) presented results in the Taurus-Auriga star forming region demonstrating that binaries with separations $\lesssim 40$ AU readily disperse protoplanetary disks. Trilling et al. (2007) used the MIPS camera on the Spitzer Space Telescope to search for infrared excess among 69 known binaries. They not only found that some binary systems have debris disks, but also that the incidence of debris disks among binaries is marginally higher than for single AFGK stars older than 600 Myr.

2. Sample

We have approached the question of stellar multiplicity among debris disk systems from a different direction than did Trilling et al. (2007). Whereas they began with a sample of known binarity, we instead selected a sample of stars with known infrared excesses that satisfy two additional criteria: ages older than 10 million years, to reduce the chances that we include protoplanetary disks, and distances within 100 parsecs, to ensure we have sufficient information. We constructed our sample from Rhee et al. (2007), Rebull et al. (2008), Chen et al. (2005), and included BD+20 307 from Song et al. (2005). We note that Mawet et al. (2011) recently demonstrated that ϵ Cephei (HIP 109857) does not contain a debris disk and is thus not included in our sample.

Many Spitzer studies tend to be biased against binaries, so we were careful to select samples that were not biased in favor or against binaries; the Rebull et al. (2008) study was based on stars in the β Pictoris moving group, while Chen et al. (2005) searched for debris disks among nearby, young (12–600 Myr) stars. For the $60\mu\text{m}$ IRAS sample from Rhee et al. (2007), we did not include objects marked as new candidate debris disks (see Note 2 in their

Table 2). By drawing from papers that use the whole sky with IRAS or in moving groups with Spitzer, we expect to avoid any significant bias in multiplicity fraction.

From these references we obtain stellar properties such as spectral type, age, fractional infrared luminosity (L_{IR}/L_*), dust temperature, and dust orbital semi-major axis. The dust properties were derived in the respective references from blackbody fits to the excess emission after modeling the stellar photosphere (however, see Section 5). We note that the infrared excesses for the sample in Trilling et al. (2007) were often faint, unlike those in our sample.

Our efforts resulted in a catalog of 112 systems with spectral types essentially in the range B8 to K2, though most are A and F-type stars (see Figure 1). Our sample, and the gathered information, is listed in Table 1. The majority of these stars are IRAS detections from Rhee et al. (2007). Many, though, have been confirmed by Spitzer. Two of our objects overlap with the Trilling et al. (2007) sample: HIP 15197 and HIP 66704. Table 1 stars have distances ranging from 3 (ϵ Eri) to 100 pc with a median distance of 38 pc.

3. Procedure

After specifying the sample, we searched the literature to determine which stars are known to be multiples. We used a variety of catalogs to search for information, including the Ninth Catalogue of Spectroscopic Binary Orbits (Pourbaix et al. 2004), the Hipparcos and Tycho Double Star catalog (ESA 1997), the Sixth Catalog of Orbits of Visual Binary Stars¹, the Washington Double Star catalog (Mason et al. 2001), the Catalog of Components of Double & Multiple stars (Dommagnet & Nys 2002), the Multiple Star Catalog (Tokovinin 1997), as well as checked SIMBAD and VizieR for papers on individual systems. While several systems have widely-separated candidate companions, most can be readily confirmed or ruled out by examining proper motions and estimated distances. Including our work in Section 4, we found 28 binary or triple star systems within the sample and list these multiples in Table 2. This corresponds to a multiplicity of $25 \pm 4\%$ (independent of whether they are binaries or triples), where the 4% error, as well as the uncertainties given in Table 3, are estimated as described by Burgasser et al. (2003). We have broken down our multiplicity fraction by spectral type in Table 3, which also includes the multiple fractions obtained by Eggleton & Tokovinin (2008) and Duquennoy & Mayor (1991). Our triples are hierarchical, with a close pair orbited by a more distant star.

We collected period and/or semi-major axis information for our multiples. Table 2 lists

¹Available at <http://ad.usno.navy.mil/wds/orb6.html>

our separations for the binary and multiple stars. For those without periods, we estimate the period assuming the projected separation is the semi-major axis and the orbits are circular. The mass of the primary is estimated from its spectral type and age. We plot all the available, or derived, periods as a histogram in Figure 2. The dashed line represents the period distribution of Duquennoy & Mayor (1991) normalized to contain about 56 systems, the expected number of multiples if the multiplicity fraction were 50%. This dashed line differs from our debris disk sample, which suggests a lack of systems with periods of about $10^2 - 10^6$ days or semi-major axes about 1–100 AU for sun-like stars.

As mentioned in Section 1, Jensen et al. (1996) found that young ($\lesssim 5$ Myr) binary stars with separations $1 < a < 50 - 100$ AU have lower sub-millimeter fluxes than more widely separated binary stars or single stars; this is approximately the same separation range as the gap in our sample and suggests that at such separations binary companions are effective at disrupting the formation of disks or accelerate the clearing of dust. However, it could also be that our sample is missing 20–30 binaries or multiples with intermediate-size semi-major axes. While most of our sample stars are well documented in the literature, there are some with very little information of the sort that can be used to determine their binary nature. We describe in the following section a search for missing companions.

4. Adaptive Optics Search for Companions

Wide separation companions would already have been detected with data from the Hipparcos satellite or proper motion surveys. To detect closer companions, one can use high-resolution spectroscopy over several epochs to see if the radial motion of the star changes indicating the presence of a massive companion. However, as most of our stars with little information are A-type stars, precise radial velocities are difficult to measure due to a relative lack of lines and rotationally-broadened profiles. An alternative way to search for companions is to use adaptive optics (AO). IRCAL, the infrared camera for adaptive optics at Lick observatory, has field of view of $20''$ and thus can detect companions out to nearly 1000 AU at 100 pc. With good seeing, companions as close as $\sim 0''.15$ can be imaged. Because the peak of the binary distribution is expected to be between 10–100 AU (Duquennoy & Mayor 1991; Eggleton & Tokovinin 2008) and our systems are located within 100 pc, IRCAL will be capable of finding these missing companions, should they exist. Roughly equal mass companions can be very quickly ruled out or confirmed after exposing for only seconds in the raw data alone. Fainter companions can be detected by co-adding dithered exposures.

We had three AO runs at Lick with IRCAL (June, October 2009; August 2010). Additional runs were scheduled in April 2010 and March 2011, but these suffered from

bad weather (rain/snow). These runs were primarily intended for observation of Herschel DEBRIS targets. DEBRIS, or Disc Emission via a Bias-free Reconnaissance in the Infrared/Submillimeter, is a Herschel key project of which we are a part (see Matthews et al. 2010). The DEBRIS project is observing 446 stars at 100 and 160- μm to look for far-infrared excesses indicative of cool dust in nearby star systems. There is some overlap between the DEBRIS sample and our own sample of 112 dusty stars and it has not been difficult to observe some additional Table 1 when the opportunity arises. Table 4 lists our IRCAL AO observations of 20 Table 1 debris disk systems. Observations were carried out using the Ks and BrG-2.16 filters. If a candidate was suspected, observations at other wavelengths (J, H, Fe II) were performed. BrG-2.16 and Fe II are narrow band filters centered on 2.167 and 1.644 μm , respectively. They are similar to the Ks and H filters, but ~ 10 times narrower.

Data reduction for these observations was carried out in the usual manner (flat fielding, dark subtraction, sky subtraction) using standard IRAF routines. Because the X and Y platescale are not the same, we used IDL routines to rescale the image while preserving flux to 76 mas/pixel in both X and Y though we later calibrate the plate scale using known binaries. In our search of these 20 systems we detected only 2 companions. One of these, HIP 35550 is a known triple system and was observed as part of the DEBRIS study. The other, HD 1051, we describe below.

4.1. HD 1051AB System

HD 1051 (HIP 1185) is a 600 Myr-old A7 star located 88.3 pc away. An infrared excess at 60 and 100 μm was detected around this star suggesting a debris disk with $T_{\text{dust}} = 40$ K and $R_{\text{dust}} = 173$ AU (Rhee et al. 2007). This system was observed as part of our IRCAL AO observations on 2010 August 4 with the Ks filter for a total integration time of 20s (10 frames, each being 10 coadds of 0.2s exposures). A candidate companion, visible in the individual frames, was detected.

To determine the projected separation for detected candidate companions, we calibrated our position angle (PA) offset and plate scale using calibrator stars from the the Sixth Catalog of Orbits of Visual Binary Stars. Some of these stars were targets in the DEBRIS project, but we used them here for calibration. We list these stars, and the results, in Table 5. We measured ΔX and ΔY , the difference in X and Y between the primary and the companion, for these stars using tasks in IRAF’s daophot package and performed a least-squares fit to:

$$\begin{aligned} \text{R.A.} &= A\Delta X \cos \theta - B\Delta Y \sin \theta \\ \text{Decl.} &= A\Delta X \sin \theta + B\Delta Y \cos \theta \end{aligned}$$

for A , B , and θ . A , B are the X, Y plate scales, respectively, and θ corresponds to the offset in position angle relative to the y-axis. The IRCAL detector is aligned such that the y-axis on image frames is approximately North, so θ amounts to a rotation. Our best fit values are: $A = 72.6$ mas/pix, $B = 77.5$ mas/pix, and $\theta = 0.52$ degrees. The rms differences in the expected position angle and separation (ρ) compared to the calculated values from our fit are adopted as our calibration uncertainties. The uncertainties in separation and position angle are 52 mas and 0.9 deg, respectively. These values are accurate only for the 2010 August observing run.

We measure the separation of HD 1051’s companion to be $7.11 \pm 0.05''$ at 311.19 ± 0.18 degrees East of North. Uncertainties are standard deviations of the measurements performed on the individual frames and do not include the calibration uncertainties. At a distance of 88.3 pc, $7.11''$ corresponds to a projected separation of 628 AU. Circular aperture photometry was likewise performed on the individual frames with a 2-pixel radius ($0''.15$) as this aperture maximized our signal-to-noise. We measure an apparent Ks magnitude difference of 5.7 ± 0.1 . At such separations, we could have detected companions up to 8 magnitudes fainter than the primary at the 5σ level, corresponding to $\sim 0.1M_{\odot}$; see Figure 3. The primary has an apparent 2MASS Ks magnitude of 6.25 ± 0.02 , which implies the secondary has apparent magnitude of 12.0 ± 0.1 , or an absolute magnitude of 7.3 ± 0.1 . The system has an estimated age of 600 Myr (Rhee et al. 2007), which implies, when comparing to Baraffe et al. (1998) models, that the secondary has spectral type $\sim M3$ and mass $\sim 0.3M_{\odot}$.

In order to confirm the detected object is bound to the system, and thus a true companion, we compare the IRCAL 2010 data with existing HST NICMOS data taken during 2007 as part of program 11157 (PI: Joseph Rhee). The HST location is $7.22 \pm 0.09''$ at 311.23 ± 0.57 degrees. As before, uncertainties are the standard deviations of multiple measurements and do not include systematics: $\sim 0.08''$ in both R.A. and Decl. due to the primary’s location behind the NICMOS coronagraphic spot. The IRCAL and HST data are displayed in Figure 4 and both show the companion at approximately the same location. Using the known distance and proper motion of the primary, as well as the measured location of the companion, we find that the secondary has not moved relative to the primary over the 3-year baseline. Figure 5 illustrates this by showing the measured location of the IRCAL and HST data and the expected motion a stationary background object would have had relative to the primary over this time period.

5. Dust Temperatures and Fractional Luminosities

Dust temperatures, and hence disk radii or semi-major axes, are estimated in the various references by fitting blackbodies to the observed infrared excess. This assumes the grains are not much smaller than the wavelengths at which they principally emit. For objects with a detected excess only at $60\mu\text{m}$, Rhee et al. (2007) assigned a temperature of 85 K corresponding to the peak of a blackbody at that wavelength in F_ν . There are about ~ 20 such objects in our sample. For objects with MIPS-measured excess emission only at $70\mu\text{m}$, Rebull et al. (2008) set a temperature of 41 K corresponding to the peak for λF_λ while Chen et al. (2005) use a temperature of 40 K, based on a modified blackbody fit to the dust around AU Mic. As most of our data come from Rhee et al. (2007), we have re-fit the spectral energy distribution (SED) for those systems with only $70\mu\text{m}$ excesses (J. Rhee, 2011, private communication). The modified objects are HIP 2072, HIP 25486, HIP 66704, and HIP 92680. In comparison, Trilling et al. (2007) determine upper limits on temperature by using the MIPS 3σ upper limit on the $24\mu\text{m}$ emission for those objects with only $70\mu\text{m}$ excesses.

For blackbody-like grains, we estimate disk semi-major axes from the stellar radius and temperature and the dust temperature:

$$R_{\text{dust}} = \frac{R_*}{2} \left(\frac{T_*}{T_{\text{dust}}} \right)^2$$

The distributions of dust temperature and fractional luminosity are shown in Figure 6. While the dust temperatures are similar for both single and multiple systems, the fractional luminosities for single stars are, on average, 2–3 times larger than those for multiple stars. We applied the Kolmogorov-Smirnov (KS) test for our sample of dust temperatures and fractional luminosities. For the dust temperature, we find $P = 0.04$, which, while small, may not allow us to rule out that they are drawn from the same distribution. However, for fractional luminosity we find $P = 2 \times 10^{-4}$ suggesting that the distribution of fractional luminosity between single and multiple stars is different.

The difference in fractional luminosity may imply that the dust is being cleared more readily in multiple systems. However, it may also be that there is a difference in the age of single and multiple systems in our sample. Older systems are known to have disks with lower fractional luminosities (Zuckerman 2001; Rhee et al. 2007; Wyatt 2008). We show the distribution of ages in Figure 7. At a glance, the figure suggests our multiples are older, which is consistent with the results in Trilling et al. (2007) in that the incidence of debris disks around multiples is marginally higher than that for single stars at ages >600 Myr.

However, closer examination (the bottom panel of Figure 7) reveals that at any given age, single stars have higher fractional luminosities than multiple stars. Hence, age alone cannot account for the lower fractional luminosities observed in multiple systems. If the incidence of dust around multiple stars relative to its incidence among single stars is in fact more likely for older stars, as suggested by our results and those of Trilling et al. (2007), then an explanation may reside in the long-term orbital stability of rocky objects. Studies have demonstrated that planetesimal orbits can be disrupted by the gravitational influence of planets in the system as they migrate (see, for example, Gomes et al. 2005; and references therein). However, as in our solar system, planetary systems should relax as they age and become progressively more dynamically quiescent. In contrast, the destabilizing influence of the gravity of stellar companions never really goes away. The very dusty system BD+20 307, where rocky planets orbits were likely altered following a Gyr of evolution, probably contains three stellar members (Zuckerman et al. 2008b).

6. Separations

While the period distribution is suggestive, it is instructive to compare the stellar separation with that of the dust’s orbital semi-major axis. As previously mentioned, all the source references for our sample calculate dust semi-major axes from fits to the spectral energy distribution (SED) assuming blackbody dust grains. Figure 8 plots the stellar separations and dust semi-major axes for Table 2 stars and those from Trilling et al. (2007). Only the shortest separation for multiples is plotted with the exception of HIP 81641, where the dust is located around the single primary. The grey region denotes dust locations that would be unstable based on the binary separation. This is adopted from Trilling et al. (2007) and is based on the stability study performed by Holman & Wiegert (1999). The stability of a test particle is defined by a critical semi-major axis, which is the maximum or minimum distance (depending on whether it’s a circumstellar or circumbinary orbit) at which a test particle survives for 10^4 times the binary period (Holman & Wiegert 1999). The stability depends on the binary mass ratio and eccentricity, but we adopt average values of 0.5 for both and use Equations 2 and 5 in Holman & Wiegert (1999) to find that the critical semi-major axis is 0.12 and 3.8 times that of the binary separation. This is comparable to the values of 0.15 and 3.5 used in Trilling et al. (2007). We note that for circular orbits, the range in critical semi-major axis is narrower: 0.27 and 2.3 times that of the binary separation, and as such we adopt the more conservative estimate with $e = 0.5$ in Figure 8. In this regime, the companion would quickly disrupt the orbits of particles be they dust or larger objects. We note that the actual boundaries of this unstable region are fuzzy for several reasons: (1) as already noted they depend on individual stellar parameters, (2) only gravitational forces are

considered (ie, no radiative effects), (3) mean-motion resonances can disrupt test particles within an ostensibly stable region, and (4) several of our systems are known triples, whereas the Holman & Wiegert (1999) study applies for binaries.

Among our sample, there are 5 binaries and 1 triple that lie in the unstable region. In addition, 3 systems from Trilling et al. (2007) lie in that region (HD 46273, HD 80671, HD 127726), as described in their paper. Those three systems (two are triples, one is a quintuple system) have detected excesses only at $70\mu\text{m}$ (in one case only marginal). The ratio of dust to star separation for these 9 systems is between about 0.3 and 2.6. These are listed in Table 6, where the separation listed for these systems is the conflicting one. As Trilling et al. (2007) suggest, these systems may be undergoing a transient event, where dust has been generated by larger objects located farther out and has now migrated inward via Poynting-Robertson drag to its observed location. In addition, both the radiation and gravity fields for triple or higher order multiples may be sufficiently complex to affect the dust temperature or orbital configuration of asteroids or planetesimals. However, we describe below a number of effects that can potentially make systems that actually are stable instead appear to be in the unstable region in Figure 8 when viewed by a distant observer.

We note that with the exception of HD 1051, the systems listed in Table 6 have infrared excesses detected at only 60 or $70\mu\text{m}$ with detections at shorter wavelengths, such as 24 and $25\mu\text{m}$, being consistent with the stellar photosphere. Cooler dust temperatures and thus larger semi-major axis are consistent with the data. For clarity in Figure 8, only systems with a single detected excess at $70\mu\text{m}$ have right pointing arrows. Ill-determined dust temperature and locations are likely to be the single most important reason for systems to lie in the unstable zone. That is, the systems may actually not be unstable: the dust may be farther away and cooler than anticipated. This would shift systems towards the right in Figure 8. Additional observations at longer wavelengths, such as with the Stratospheric Observatory for Infrared Astronomy (SOFIA) and the Herschel Space Observatory, will be key in determining temperatures for these systems.

An additional potential source of error in the horizontal placement of systems in Figure 8 is the assumption of blackbody grains. Small grains radiate inefficiently and, at a given distance from a star, will have higher temperatures than blackbody grains (Zuckerman 2001; and references therein). As such, at a given temperature small grains will be located further to the right on the Figure 8 horizontal axis than will blackbody grains. A handful of systems have been resolved in thermal emission (where the dust particles themselves radiate at wavelengths between 20 and $1000\mu\text{m}$), or in scattered light, where small grains reflect and scatter light from the central star. We consider these systems in Table 7 and Figure 9, noting that a handful of known resolved systems are not listed. These include β Pic, τ Ceti, γ Oph,

and ζ^2 Ret, as either too little information is available or, in β Pic’s case, too much, and thus meaningful determination of a characteristic resolved radius is not possible. Note that HD 141569A and HD 98800B appear in Table 7; these usually have been classified as transition disks. For Table 7 and Figure 9 we use an average for the range in location of the dust or adopt the location of peak emission. Because grain semi-major axes plotted in Figure 8 are based on thermal emission, the relevant comparison of semi-major axes in Table 7 and Figure 9 is with spatially resolved thermal emission and not with scattered light. Thermally resolved disk radii range from one to five times larger than expected from blackbody-fit radii and likely are due to the particular composition, size, and porosity of grains in the disk. For actual disk semi-major axes 5 times larger than the blackbody model, one can shift at most 5 systems out of 9 from the unstable region in Figure 8. Hence consideration of the actual sizes of disks would result in shifting a few systems to the right (larger disk radii) and into stability. Similar considerations could shift a few apparently stable systems into an unstable configuration.

Because of projection effects and location along the orbit, the observed binary separation is a lower limit and could be somewhat larger than that plotted in Figure 8. The ratio between projected separation (ρ) and semi-major axis (a) for a circular orbit is:

$$\rho = a\sqrt{1 - \sin^2 \omega \sin^2 i}$$

where ω is the location along the orbit and thus has a total range of 0 to 2π (from Macintosh 1994; however, see also Leinert et al. 1993). The inclination, i , has a range of 0 to $\pi/2$ ($i = 0$ denotes a face-on orbit). We can estimate the average ratio:

$$\left\langle \frac{\rho}{a} \right\rangle = \frac{\int_0^{\pi/2} \int_0^{2\pi} \sqrt{1 - \sin^2 \omega \sin^2 i} \, did\omega}{\int_0^{\pi/2} \int_0^{2\pi} \, did\omega} \approx 0.842 \approx \frac{1}{1.19}$$

So the average binary separation could be $\sim 20\%$ larger than what is actually measured. However, on an individual-case basis, objects may have inclinations and orbit locations such that objects move outside the unstable region. We generated 100,000 random inclinations between 0 and 90° and orbit locations between 0 and 360° to compute the ratio of projected to actual separation. This distribution is integrated and normalized in order to estimate how often ratios lower than a particular value appear. For the unstable systems listed in Table 6, we estimate what semi-major axis is required to yield a dust radius-to-star separation ratio of 0.12 and calculate the probability (the final column) of achieving stability in Figure 8 based on the measured stellar separation. In all cases the likelihood is low that the semi-major axis of the binary system is much larger than the observed binary separation. Thus, at most

one unstable disk system would be shifted upward in Figure 8 into a stable configuration. However, as noted in the first paragraph of the present Section, Figure 8 assumes a binary eccentricity of 0.5. If the HD 1051 binary were instead to have a circular orbit, then the probability that the orbiting dust is stable would be 60%. In addition, should the HIP 76127 binary also possess a circular orbit, then the circumbinary dust would be stable as its dust radius-to-star separation ratio is larger than the critical semi-major axis for circular orbits (2.3). In practice, as most binary orbits are eccentric, the companion will spend more time away from the primary, resulting in a lower ratio between projected separation and semi-major axis than the average estimated here.

Summarizing the above considerations, data points in Figure 8 may be shifted as a result of incorrect temperature determination, dust grain characteristics, and projection effects. The dominant effect in our sample is likely the incorrect determination of dust temperatures, and thus, of dust semi-major axes. The other two effects are, in general, probably insufficient to shift all systems outside the region where dust particle orbits are expected to be unstable. The result of binary interactions in the disks will be to either to clear gaps or to truncate the disks (Lubow & Artymowicz 2000; Artymowicz & Lubow 1994). The small number of these disk systems in the unstable zone suggests that binaries, although they can form disks, are more likely to disrupt the formation and evolution of planetary systems when their separations are comparable to typical disk sizes.

7. Disk Masses

A final comparison one can make for our debris disk sample are dust masses determined from (sub)millimeter photometry. Nilsson et al. (2010) have summarized all submm and longer wavelength detections of debris disks, but only briefly comment on binarity in their paper. We have compared our sample to their list, but only 23 of our debris disks have submm or mm measurements. Of those 23 only 3 are binaries and thus our comparisons are limited by small number statistics. Disk dust masses can be readily estimated with:

$$M_d = \frac{S_\nu D^2}{k_\nu B_\nu(T_d)}$$

where S_ν is the submm flux, D is the distance between the dust and Earth, and B_ν is the blackbody flux at the dust temperature T_d . The dust opacity, k_ν , is extrapolated from an opacity of $1.7 \text{ cm}^2 \text{ g}^{-1}$ at $880 \mu\text{m}$ assuming a dust opacity slope $\beta=1$: $k_\nu = 1.7(880/\lambda)^\beta$ (see Zuckerman et al. 2008a).

We list our estimated disk dust masses in Table 8. The average dust mass for our 20 single stars is ~ 7 Moon masses (M_{Moon} ; the median is $\sim 3 M_{\text{Moon}}$). In contrast, our 3

binary star systems have an average disk mass of $\sim 0.7 M_{\text{Moon}}$. These single and binary star dust masses, while few, are consistent with our results for fractional luminosities and dust separations. That is, binaries or multiples are more effective at clearing their disks and as such, they possess lower disk masses (as previously found for very young systems; see Jensen et al. 1996). We note, however, that these few binaries have ages ≥ 200 Myr, whereas our single stars are predominantly younger than ~ 200 Myr. Hence, this disk mass difference, while suggestive, must be taken with care.

Further submm and mm observations of our debris disk sample, for example with JCMT, APEX, or ALMA, will be key in gathering a larger sample of disk mass measurements for both single and multiple debris disk systems. In particular, for the systems in the unstable region of Figure 8, we extrapolate what flux density is expected at $850\mu\text{m}$. We use the systems measured by Williams & Andrews (2006) and compare the F_{850}/F_{60} ratio as a function of dust temperature in order to estimate F_{850} . We find that our unstable disks listed in Table 6 (not including the three Trilling et al. 2007 systems), are anticipated to have flux densities of $\sim 1 - 10$ mJy at $850\mu\text{m}$. In addition, these systems should have angular radii (from the SED fits) of $\sim 0.4 - 4''$. In a single hour, at 345 GHz with a $1''$ beam, full ALMA (54 antennae) can reach sensitivities of ~ 0.02 mJy/beam, making systems like these readily detectable and resolvable.

8. Conclusions

We find that the fraction of stars in binary or multiple systems among our debris disk systems is $25 \pm 4\%$. This is less than the anticipated $\sim 1/2$ of multiple stars and could be due either to a physical difference (ie, less multiples among debris disk systems) or to incomplete multiplicity data for some of our stars. We performed an adaptive optics search on 20 not previously well-studied systems in order to search for binaries in the 10–1000 AU separation range. We discovered only a single binary: HD 1051, an A-star with an M-star companion with projected separation of 628 AU. The distribution of systems in stellar separation vs. blackbody dust semi-major axis confirms the theoretical expectation that dust will not form or survive at separations comparable to that of the semi-major axis of the secondary star. Additionally, the fractional luminosities and disk masses, the latter inferred from a handful of submm detections, are lower for the multiples systems; this serves to strengthen the idea that these systems clear out their disks more effectively than do single stars.

What does this imply for planet formation? First, many binaries do possess disks and as such could very well form planets. However, our results suggest that binaries are less likely to possess long-lived, massive disks. We infer this by our result of fewer than expected binaries

in our sample and the lower disk masses and fractional luminosities among the binaries. The fact that the binary semi-major axis distribution peaks around ~ 30 AU (Duquennoy & Mayor 1991) suggests that most binaries will only rarely form planets at semi-major axes comparable to the gas giants in our own solar system. For a binary to possess planets it must either be a very widely separated binary with planets orbiting a single star (in fact, $\sim 20\%$ of known extrasolar planets are in such systems; see Raghavan et al. 2006) or it must be a very closely separated binary with planets forming in a massive circumbinary disk.

Results from unbiased Herschel surveys followed by ALMA imaging should address uncertainties associated with Figures 8 and 9 of the present study.

We thank Gaspard Duchene and Harold Butner for useful discussions and for allowing us to observe some Table 1 systems in our joint observing runs. Many thanks to Sasha Hinkley and Lewis Roberts for double checking our targets with their binary program, to Marshall Perrin for his IDL IRCAL routines, and to Joseph Rhee for assistance with determining dust temperatures. We thank our referee, Michal Simon, for a prompt review and constructive suggestions. This research has made use of the Washington Double Star Catalog maintained at the U.S. Naval Observatory, and the SIMBAD database and the VizieR catalog access tool, operated at CDS, Strasbourg, France. This research was supported in part by NASA grants to UCLA.

REFERENCES

- Alzner, A. 1998, *A&AS*, 132, 237
- Andrews, S. M., Czekala, I., Wilner, D. J., Espaillat, C., Dullemond, C. P., & Hughes, A. M. 2010, *ApJ*, 710, 462
- Artymowicz, P., & Lubow, S. H. 1994, *ApJ*, 421, 651
- Baraffe, I., Chabrier, G., Allard, F., & Hauschildt, P. H. 1998, *A&A*, 337, 403
- Barrado y Navascues, D., Stauffer, J. R., Hartmann, L., & Balachandran, S. C. 1997, *ApJ*, 475, 313
- Batten, A. H., Fletcher, J. M., & Mann, P. J. 1978, *Publications of the Dominion Astrophysical Observatory Victoria*, 15, 121
- Beuermann, K., et al. 2010, *A&A*, 521, L60

- Biller, B. A., et al. 2010, *ApJ*, 720, L82
- Borucki, W. J., et al. 2011, arXiv:1102.0541
- Bouwman, J., Lawson, W. A., Dominik, C., Feigelson, E. D., Henning, T., Tielens, A. G. G. M., & Waters, L. B. F. M. 2006, *ApJ*, 653, L57
- Brendley, M., & Hartkopf, W. I. 2007, *IAU Commission on Double Stars*, 163
- Burgasser, A. J., Kirkpatrick, J. D., Reid, I. N., Brown, M. E., Miskey, C. L., & Gizis, J. E. 2003, *ApJ*, 586, 512
- Chen, C. H., et al. 2005, *ApJ*, 634, 1372
- Chen, C. H., Sheehan, P., Watson, D. M., Manoj, P., & Najita, J. R. 2009, *ApJ*, 701, 1367
- Churcher, L., Wyatt, M., & Smith, R. 2011, *MNRAS*, 410, 2
- Cieza, L. A., et al. 2009, *ApJ*, 696, L84
- Corder, S., et al. 2009, *ApJ*, 690, L65
- Cvetkovic, Z., & Ninkovic, S. 2010, *Serbian Astronomical Journal*, 180, 71
- Deeg, H. J., Ocaña, B., Kozhevnikov, V. P., Charbonneau, D., O'Donovan, F. T., & Doyle, L. R. 2008, *A&A*, 480, 563
- Dommanget, J., & Nys, O. 2002, *VizieR Online Data Catalog*, 1274, 0
- Doyle, L. R., Carter, J. A., Fabrycky, D. C., et al. 2011, *Science*, 333, 1602
- Duquennoy, A., & Mayor, M. 1991, *A&A*, 248, 485
- Eggenberger, A., Udry, S., Chauvin, G., Beuzit, J.-L., Lagrange, A.-M., Ségransan, D., & Mayor, M. 2007, *A&A*, 474, 273
- Eggleton, P. P., & Tokovinin, A. A. 2008, *MNRAS*, 389, 869
- Eker, Z., et al. 2008, *MNRAS*, 389, 1722
- ESA. 1997, *VizieR Online Data Catalog*, 1239, 0
- Fitzgerald, M. P., Kalas, P. G., Duchene, G., Pinte, C., & Graham, J. R. 2007, *ApJ*, 670, 536
- Golimowski, D. A., et al. 2011, *AJ*, 142, 30

- Gomes, R., Levison, H. F., Tsiganis, K., & Morbidelli, A. 2005, *Nature*, 435, 466
- Gould, A., & Chanamé, J. 2004, *ApJS*, 150, 455
- Greaves, J. S., et al. 1998, *ApJ*, 506, L133
- Haisch, K. E., Lada, E. A., & Lada, C. J. 2001, *ApJ*, 553, L153
- Hillenbrand, L. A., et al. 2008, *ApJ*, 677, 630
- Hines, D. C., et al. 2007, *ApJ*, 671, L165
- Holman, M. J., & Wiegert, P. A. 1999, *AJ*, 117, 621
- Jensen, E. L. N., Mathieu, R. D., & Fuller, G. A. 1996, *ApJ*, 458, 312
- Kalas, P., Liu, M. C., & Matthews, B. C. 2004, *Science*, 303, 1990
- Kalas, P., Graham, J. R., & Clampin, M. 2005, *Nature*, 435, 1067
- Kalas, P., Graham, J. R., Clampin, M. C., & Fitzgerald, M. P. 2006, *ApJ*, 637, L57
- Kalas, P., Fitzgerald, M. P., & Graham, J. R. 2007a, *ApJ*, 661, L85
- Kalas, P., Duchene, G., Fitzgerald, M. P., & Graham, J. R. 2007b, *ApJ*, 671, L161
- Konacki, M., Muterspaugh, M. W., Kulkarni, S. R., & Helminiak, K. G. 2009, *ApJ*, 704, 513
- Kraus, A. L., Ireland, M. J., Hillenbrand, L. A., & Martinache, F. 2011, arXiv:1109.4141
- Krist, J. E., et al. 2005, *AJ*, 129, 1008
- . 2010, *AJ*, 140, 1051
- Lee, J. W., Kim, S., Kim, C., Koch, R. H., Lee, C., Kim, H., & Park, J. 2009, *AJ*, 137, 3181
- Leinert, C., Zinnecker, H., Weitzel, N., et al. 1993, *A&A*, 278, 129
- Liseau, R., et al. 2010, *A&A*, 518, L132+
- Low, F. J., Smith, P. S., Werner, M., Chen, C., Krause, V., Jura, M., & Hines, D. C. 2005, *ApJ*, 631, 1170
- Lubow, S. H., & Artymowicz, P. 2000, *Protostars and Planets IV* (Book - Tucson: University of Arizona Press; eds Mannings, 731
- Luu, J. X., & Jewitt, D. C. 2002, *ARA&A*, 40, 63

- Macintosh, B. A. 1994, Ph.D. Thesis, University of California, Los Angeles
- Mason, B. D., Wycoff, G. L., Hartkopf, W. I., Douglass, G. G., & Worley, C. E. 2001, *AJ*, 122, 3466
- Mason, B. D., Hartkopf, W. I., Gies, D. R., Henry, T. J., & Helsel, J. W. 2009, *AJ*, 137, 3358
- . 2011, *VizieR Online Data Catalog*, 1, 2026
- Matthews, B. C., et al. 2010, *A&A*, 518, L135+
- Mawet, D., Mennesson, B., Serabyn, E., Stapelfeldt, K., & Absil, O. 2011, arXiv:1107.3872
- Moerchen, M. M., Telesco, C. M., De Buizer, J. M., Packham, C., & Radomski, J. T. 2007, *ApJ*, 666, L109
- Nilsson, R., et al. 2010, *A&A*, 518, A40
- Pourbaix, D. 2000, *A&AS*, 145, 215
- Pourbaix, D., et al. 2004, *A&A*, 424, 727
- Raghavan, D., Henry, T. J., Mason, B. D., Subasavage, J. P., Jao, W.-C., Beaulieu, T. D., & Hambly, N. C. 2006, *ApJ*, 646, 523
- Raghavan, D., et al. 2010, *ApJS*, 190, 1
- Rebull, L. M., et al. 2008, *ApJ*, 681, 1484
- Reid, I. N., Cruz, K. L., & Allen, P. R. 2007, *AJ*, 133, 2825
- Rhee, J. H., Song, I., Zuckerman, B., & McElwain, M. 2007, *ApJ*, 660, 1556
- Samus, N. N., Durlevich, O. V., & et al. 2009, *VizieR Online Data Catalog*, 1
- Schneider, G., et al. 1999, *ApJ*, 513, L127
- . 2006, *ApJ*, 650, 414
- Shatskii, N. I. 1998, *Astronomy Letters*, 24, 257
- Sibthorpe, B., et al. 2010, *A&A*, 518, L130+
- Smith, R., Churcher, L. J., Wyatt, M. C., Moerchen, M. M., & Telesco, C. M. 2009, *A&A*, 493, 299

- Song, I., Zuckerman, B., Weinberger, A. J., & Becklin, E. E. 2005, *Nature*, 436, 363
- Su, K. Y. L., et al. 2006, *ApJ*, 653, 675
- Su, K. Y. L., et al. 2009, *ApJ*, 705, 314
- Tokovinin, A. A. 1997, *A&AS*, 124, 75
- Torres, C. A. O., Quast, G. R., Melo, C. H. F., & Sterzik, M. F. 2008, *Handbook of Star Forming Regions, Volume II*, 757
- Trilling, D. E., et al. 2007, *ApJ*, 658, 1289
- Uzpen, B., Kobulnicky, H. A., & Kinemuchi, K. 2009, *AJ*, 137, 3329
- Weinberger, A. J., Becklin, E. E., Schneider, G., Smith, B. A., Lowrance, P. J., Silverstone, M. D., Zuckerman, B., & Terrile, R. J. 1999, *ApJ*, 525, L53
- Weinberger, A. J. 2008, *ApJ*, 679, L41
- Weinberger, A. J., Becklin, E. E., Song, I., & Zuckerman, B. 2011, *ApJ*, 726, 72
- Williams, J. P., & Andrews, S. M. 2006, *ApJ*, 653, 1480
- Wyatt, M. C. 2008, *ARA&A*, 46, 339
- Zuckerman, B. 2001, *ARA&A*, 39, 549
- Zuckerman, B., & Song, I. 2004, *ARA&A*, 42, 685
- Zuckerman, B., et al. 2008a, *ApJ*, 683, 1085
- Zuckerman, B., Fekel, F. C., Williamson, M. H., Henry, G. W., & Munro, M. P. 2008b, *ApJ*, 688, 1345

Table 1. Debris Disk Sample

Name	HIP Number	Spectral Type	Dist. (pc)	Detection	T_{dust} (K)	L_{IR}/L_{\star}	R_{dust} (AU)	Multiple?	Age (Myr)	References
HR 9	HIP 560	F2	39.1	MIPS	120	1.0E-04	10	N	12	Rebull et al. 2008
HD 432	HIP 746	F2	16.7	IRAS	120	2.5E-05	28	N	1000	Rhee et al. 2007
HD 1051	HIP 1185	A7	88.3	IRAS	40	4.3E-04	173	Y	600	Rhee et al. 2007
HD 2262	HIP 2072	A5	24	MIPS ^a	140	1.1E-05	14	N	200	Chen et al. 2005
HD 6798	HIP 5626	A3	83.5	IRAS	75	1.5E-04	93	N	200	Rhee et al. 2007
HD 8538	HIP 6686	A5	30.5	IRAS	85	6.0E-06	88	Y	600	Rhee et al. 2007
HD 8907	HIP 6878	F8	34.2	IRAS/MIPS/ISO	45	2.1E-04	59	N	200	Rhee et al. 2007
HD 9672	HIP 7345	A1	61.3	IRAS	80	7.9E-04	60	N	20	Rhee et al. 2007
HD 10472	HIP 7805	F2	66.6	IRAS/MIPS	70	3.7E-04	30	N	30	Rhee et al. 2007
HD 10647	HIP 7978	F8	17.4	IRAS	65	4.2E-04	22	N	300	Rhee et al. 2007
HD 10638	HIP 8122	A3	71.7	IRAS	85	4.7E-04	33	N	100	Rhee et al. 2007
HD 10939	HIP 8241	A1	57	IRAS/MIPS	75	6.4E-05	80	N	200	Rhee et al. 2007
BD +20 307	HIP 8920	G0	91.9	IRAS/Gemini/Keck	358	3.2E-02	0.85	Y	1000	Song et al. 2005; Weinberger et al. 2011
HD 14055	HIP 10670	A1	36.1	IRAS	75	7.2E-05	80	N	100	Rhee et al. 2007
HIP 10679	HIP 10679	G2	34	MIPS	100	8.0E-04	20	Y	12	Rebull et al. 2008
HD 15115	HIP 11360	F2	44.8	IRAS/MIPS/ISO	65	5.1E-04	35	N	100	Rhee et al. 2007
AG Tri	HIP 11437	K8	42.3	MIPS	65	7.9E-04	10	Y	12	Rebull et al. 2008
HD 15745	HIP 11847	F0	63.7	IRAS/MIPS/ISO	85	1.7E-03	22	N	30	Rhee et al. 2007
HD 16743	HIP 12361	F1	60	IRAS/MIPS	40	5.9E-04	119	N	200	Rhee et al. 2007
HD 17390	HIP 12964	F3	45.1	IRAS/MIPS	55	2.0E-04	55	N	300	Rhee et al. 2007
HD 17848	HIP 13141	A2	50.7	IRAS/MIPS	55	6.4E-05	97	N	100	Rhee et al. 2007
HD 19356	HIP 14576	B8	28.5	IRAS/MIPS	250	1.7E-05	13	Y	300	Rhee et al. 2007
HD 20320	HIP 15197	A5	36.8	IRAS/MIPS	95	2.5E-05	31	Y	400	Su et al. 2006; Rhee et al. 2007
HD 21997	HIP 16449	A3	73.8	IRAS/MIPS	60	4.9E-04	82	N	50	Rhee et al. 2007
ϵ Eri	HIP 16537	K2	3.2	IRAS/MIPS/ISO	40	8.3E-05	27	N	730	Rhee et al. 2007
HD 25457	HIP 18859	F5	19.2	IRAS/MIPS/ISO	85	1.3E-04	16	N	30	Rhee et al. 2007
HD 27290	HIP 19893	F4	20.3	IRAS	80	2.3E-05	31	N	300	Rhee et al. 2007
HD 30447	HIP 22226	F3	78.1	IRAS/MIPS	65	8.9E-04	37	N	100	Rhee et al. 2007
HD 31295	HIP 22845	A0	37	IRAS/MIPS	80	8.4E-05	49	N	100	Rhee et al. 2007
HD 34324	HIP 24528	A3	85.8	IRAS	100	1.7E-04	28	N	200	Rhee et al. 2007
HR 1817	HIP 25486	F7	26.8	MIPS ^a	80	3.6E-05	17	Y	12	Rebull et al. 2008
HD 37484	HIP 26453	F3	59.5	IRAS/MIPS	90	2.9E-04	19	N	30	Rhee et al. 2007
HD 38206	HIP 26966	A0	69.2	IRAS/MIPS	85	2.0E-04	53	N	50	Rhee et al. 2007
HD 38393	HIP 27072	F7	9	IRAS/MIPS	90	7.7E-06	15	Y	1000	Rhee et al. 2007

Table 1—Continued

Name	HIP Number	Spectral Type	Dist. (pc)	Detection	T_{dust} (K)	L_{IR}/L_*	R_{dust} (AU)	Multiple?	Age (Myr)	References
HD 38678	HIP 27288	A2	21.5	IRAS/MIPS	220	1.3E-04	6	N	100	Rhee et al. 2007
β Pic	HIP 27321	A3	19.3	IRAS/MIPS	110	2.6E-03	19	N	12	Rhee et al. 2007
HD 40136	HIP 28103	F1	15	IRAS/MIPS	185	2.0E-05	6	N	300	Rhee et al. 2007
HD 48682	HIP 32480	G0	16.5	IRAS/MIPS	60	8.9E-05	29	N	600	Rhee et al. 2007
HD 50571	HIP 32775	F7	33.2	IRAS/MIPS	45	1.6E-04	68	N	300	Rhee et al. 2007
HD 53143	HIP 33690	K0	18.4	IRAS/MIPS	80	2.0E-04	9	N	300	Rhee et al. 2007
HD 54341	HIP 34276	A0	92.9	IRAS	85	2.0E-04	51	N	10	Rhee et al. 2007
HD 56986	HIP 35550	F0	18	IRAS/MIPS	60	8.9E-06	71	Y	400	Rhee et al. 2007
HD 61005	HIP 36948	G3	34.5	IRAS/MIPS	60	2.6E-03	16	N	100	Rhee et al. 2007
HD 67523	HIP 39757	F2	19.2	IRAS	85	5.4E-06	50	N	2000	Rhee et al. 2007
HD 70313	HIP 41152	A3	51.4	IRAS/MIPS	80	5.2E-05	56	N	200	Rhee et al. 2007
HD 71155	HIP 41307	A0	38.3	IRAS/MIPS	130	4.1E-05	29	N	100	Rhee et al. 2007
HD 73752	HIP 42430	G3	19.9	IRAS	80	3.2E-05	21	Y	600	Rhee et al. 2007
HD 76582	HIP 44001	F0	49.3	IRAS	85	2.2E-04	35	N	300	Rhee et al. 2007
HD 84870	HIP 48164	A3	89.5	IRAS	85	5.5E-04	32	N	100	Rhee et al. 2007
HD 85672	HIP 48541	A0	93.1	IRAS	85	4.8E-04	32	N	30	Rhee et al. 2007
HD 91375	HIP 51438	A2	79.4	IRAS	85	2.4E-05	99	N	400	Rhee et al. 2007
HD 91312	HIP 51658	A7	34.3	IRAS	40	1.1E-04	179	N ^b	200	Rhee et al. 2007
HD 92945	HIP 52462	K1	21.6	IRAS/MIPS	45	6.7E-04	23	N	100	Rhee et al. 2007
HD 95418	HIP 53910	A1	24.3	IRAS	120	1.2E-05	45	N	500	Rhee et al. 2007
HD 99945	HIP 56253	A2	59.8	IRAS	85	1.0E-04	37	N	300	Rhee et al. 2007
HD 102647	HIP 57632	A3	11.1	IRAS/MIPS	160	4.3E-05	11	Y	50	Rhee et al. 2007
HD 107146	HIP 60074	G2	28.5	IRAS/MIPS	55	9.5E-04	29	N	100	Rhee et al. 2007
η Crv	HIP 61174	F2	18.2	IRAS/MIPS	180	1.2E-04	5	N	300	Rhee et al. 2007
HD 110058	HIP 61782	A0	99.9	IRAS/IRS	130	2.5E-03	11	N	10	Rhee et al. 2007
HD 110411	HIP 61960	A0	36.9	IRAS/MIPS	85	6.2E-05	38	N	100	Rhee et al. 2007
HD 112429	HIP 63076	F0	29	MIPS	100	2.4E-05	20	N	50	Chen et al. 2005
HD 113337	HIP 63584	F6	37.4	IRAS	100	1.0E-04	18	Y	50	Rhee et al. 2007
HD 115116	HIP 64921	A7	85.4	IRAS	80	3.4E-04	39	N	100	Rhee et al. 2007
HD 119124	HIP 66704	F7	25	MIPS ^e	55	4.0E-05	32	Y	200	Chen et al. 2005
HD 121384	HIP 68101	G8	38.1	IRAS	45	2.5E-04	91	N	3000	Rhee et al. 2007
HD 122652	HIP 68593	F8	37.2	IRAS/MIPS	60	1.4E-04	28	N	300	Rhee et al. 2007
HD 124718	HIP 69682	G5	61.3	IRAS	85	2.1E-03	10	N	500	Rhee et al. 2007
HD 125162	HIP 69732	A0	29.8	IRAS/MIPS	100	5.2E-05	32	N	200	Rhee et al. 2007

Table 1—Continued

Name	HIP Number	Spectral Type	Dist. (pc)	Detection	T_{dust} (K)	L_{IR}/L_*	R_{dust} (AU)	Multiple?	Age (Myr)	References
HD 125473	HIP 70090	A0	75.8	IRAS	120	2.1E-05	64	Y	300	Rhee et al. 2007
HD 126265	HIP 70344	G2	70.1	IRAS	85	3.9E-04	26	N	500	Rhee et al. 2007
HD 127821	HIP 70952	F4	31.7	IRAS	50	2.6E-04	55	N	200	Rhee et al. 2007
HD 127762	HIP 71075	A7	26.1	IRAS	55	1.0E-05	151	Y	1000	Rhee et al. 2007
σ Boo	HIP 71284	F3	15.5	IRAS/MIPS/ISO	40	4.9E-06	88	N	1000	Rhee et al. 2007
HD 135502	HIP 74596	A2	69.4	IRAS	65	3.3E-05	123	N	200	Rhee et al. 2007
HD 135382	HIP 74946	A1	56	IRAS	50	9.3E-06	481	N	700	Rhee et al. 2007
HD 138749	HIP 76127	B6	95.3	IRAS	75	2.0E-05	171	Y	200	Rhee et al. 2007
HD 139006	HIP 76267	A0	22.9	IRAS/MIPS	190	2.4E-05	17	Y	500	Rhee et al. 2007
HD 139590	HIP 76635	G0	55.1	IRAS	85	3.9E-04	17	N	5000	Rhee et al. 2007
HD 139664	HIP 76829	F5	17.5	IRAS/MIPS	75	1.2E-04	25	N	200	Rhee et al. 2007
HD 143894	HIP 78554	A3	54.3	IRAS	45	4.6E-05	211	N	300	Rhee et al. 2007
HD 149630	HIP 81126	B9	92.7	IRAS	80	3.0E-05	157	Y	700	Rhee et al. 2007
HD 150378	HIP 81641	A1	92.9	IRAS	95	1.2E-04	57	Y	200	Rhee et al. 2007
HD 151044	HIP 81800	F8	29.4	IRAS/MIPS/ISO	55	8.3E-05	35	N	500	Rhee et al. 2007
HD 154145	HIP 83480	A2	94.9	IRAS	85	4.3E-04	45	N	300	Rhee et al. 2007
HD 157728	HIP 85157	F0	42.8	IRAS	90	2.7E-04	30	N	100	Rhee et al. 2007
HD 158352	HIP 85537	A8	63.1	IRAS/MIPS	70	6.8E-05	85	N	600	Rhee et al. 2007
HD 161868	HIP 87108	A0	29.1	IRAS/MIPS	85	7.8E-05	54	N	200	Rhee et al. 2007
HD 162917	HIP 87558	F4	31.4	IRAS	85	2.5E-04	20	N	400	Rhee et al. 2007
HD 164249	HIP 88399	F5	46.9	IRAS/MIPS/ISO	70	1.0E-03	27	N	12	Rhee et al. 2007
HD 169022	HIP 90185	B9	44.3	IRAS	100	4.5E-06	155	Y	300	Rhee et al. 2007
HD 170773	HIP 90936	F5	36.1	IRAS/MIPS/ISO	50	4.6E-04	61	N	200	Rhee et al. 2007
Vega	HIP 91262	A0	7.8	IRAS/MIPS	80	2.1E-05	93	N	220	Rhee et al. 2007
HD 172555	HIP 92024	A7	29.2	IRAS/MIPS	320	8.1E-04	2	Y	12	Rhee et al. 2007
PZ Tel	HIP 92680	K0	49.7	MIPS ^a	85	9.4E-05	11	Y	12	Rebull et al. 2008
HD 176638	HIP 93542	A0	56.3	IRAS	120	9.7E-05	34	N	200	Rhee et al. 2007
η Tel	HIP 95261	A0	47.7	IRAS/MIPS/ISO	150	2.1E-04	15	Y	12	Rhee et al. 2007
HD 181327	HIP 95270	F5	50.6	IRAS/MIPS	75	3.5E-03	25	N	12	Rhee et al. 2007
HD 182681	HIP 95619	B8	69.1	IRAS	85	2.0E-04	55	N	50	Rhee et al. 2007
HD 191089	HIP 99273	F5	53.5	IRAS/MIPS	95	1.4E-03	15	N	30	Rhee et al. 2007
HD 191692	HIP 99473	B9	88	IRAS	85	6.6E-06	213	Y	500	Rhee et al. 2007
HD 195627	HIP 101612	F1	27.6	IRAS/MIPS	65	1.1E-04	51	N	200	Rhee et al. 2007
HD 196544	HIP 101800	A2	54.3	IRAS/MIPS	100	3.9E-05	31	Y	30	Rhee et al. 2007

Table 1—Continued

Name	HIP Number	Spectral Type	Dist. (pc)	Detection	T_{dust} (K)	L_{IR}/L_*	R_{dust} (AU)	Multiple?	Age (Myr)	References
AU Mic	HIP 102409	M1	9.9	IRAS/MIPS	50	3.6E-04	9	N	12	Rhee et al. 2007
HD 205674	HIP 106741	F3	52.6	IRAS	85	4.0E-04	20	N	300	Rhee et al. 2007
HD 205536	HIP 107022	G8	22.1	IRAS	80	2.9E-04	10	N	500	Rhee et al. 2007
HD 206893	HIP 107412	F5	38.9	IRAS/MIPS/ISO	55	2.7E-04	41	N	200	Rhee et al. 2007
HD 207129	HIP 107649	G2	15.6	IRAS/MIPS/ISO	55	1.2E-04	27	Y	600	Rhee et al. 2007
HD 209253	HIP 108809	F6	30.1	IRAS/MIPS/ISO	75	7.3E-05	18	N	200	Rhee et al. 2007
HD 213617	HIP 111278	F1	52.9	IRAS/MIPS	55	9.4E-05	69	N	600	Rhee et al. 2007
Fomalhaut	HIP 113368	A3	7.7	IRAS/MIPS	65	8.0E-05	73	Y	220	Rhee et al. 2007
HD 218396	HIP 114189	A5	39.9	IRAS/ISO	50	2.3E-04	77	N	30	Rhee et al. 2007
HD 221853	HIP 116431	F0	71.2	IRAS/MIPS/ISO	85	7.4E-04	26	N	100	Rhee et al. 2007

Note. — List of all debris disks stars in our sample. R_{dust} is the disk radius for blackbody grains (see Section 5).

^a— T_{dust} , L_{IR}/L_* , and R_{dust} have been modified from those given in the cited references so that the peak of the blackbody fit lies at the MIPS $70\mu\text{m}$ detection (see Section 5 for more details).

^b— While HIP 51658 is listed in the 7th spectroscopic binary orbit catalog with a period of 292.56 days (Batten et al. 1978), the quality flag is set to the lowest value indicating the binary nature is in question. More recent catalogs (see Pourbaix et al. 2004) no longer list this system.

Table 2. Multiples in Debris Disk Sample

Name	Spectral Type	Dist. (pc)	R_{dust} (AU)	S1 (AU)	S2 (AU)	P1 (days)	P2 (days)	References
HIP 1185	A7	88.3	173	626.9	...	4.27E+06	...	this work
HIP 6686	A5	30.5	88	2.1	...	7.59E+02	...	Eggleton & Tokovinin 2008; Samus et al. 2009
HIP 8920	G0	91.9	0.85	0.047	...	3.45E+00	...	Weinberger 2008
HIP 10679	G2	34	20	471.9	...	3.06E+06	...	ESA 1997
HIP 11437 ^a	K8	42.3	10	1015.2	...	1.18E+07	...	Zuckerman & Song 2004; Mason et al. 2011
HIP 14576	B8	28.5	13	0.07	3.0	2.87E+00	6.80E+02	Pourbaix et al. 2004; Eggleton & Tokovinin 2008; Tokovinin 1997
HIP 15197	A5	36.8	31	0.17	...	1.79E+01	...	Pourbaix et al. 2004; Eggleton & Tokovinin 2008; Trilling et al. 2007
HIP 25486	F7	26.8	18.9	0.021	...	9.00E-01	...	Eker et al. 2008
HIP 27072	F7	9	15	866.3	...	8.17E+06	...	Gould & Chanamé 2004; Eggleton & Tokovinin 2008
HIP 35550	F0	18	71	3.9	125.6	2.24E+03	4.37E+05	Pourbaix et al. 2004; Eggleton & Tokovinin 2008; Tokovinin 1997
HIP 42430	G3	19.9	21	34.0	...	4.49E+04	...	ESA 1997; Eggleton & Tokovinin 2008; Raghavan et al. 2010
HIP 57632	A3	11.1	11	440.7	...	2.39E+06	...	Eggleton & Tokovinin 2008
HIP 63584	F6	37.4	18	4450.6	...	9.51E+07	...	Reid et al. 2007; Mason et al. 2001
HIP 66704	F7	25	31.9	440.0	...	2.96E+06	...	Duquenooy & Mayor 1991
HIP 70090	A0	75.8	64	0.33	...	3.88E+01	...	Eggleton & Tokovinin 2008
HIP 71075	A7	26.1	151	1.8	...	6.72E+02	...	Eggleton & Tokovinin 2008
HIP 76127	B6	95.3	171	66.3	...	8.06E+04	...	ESA 1997; Alzner 1998
HIP 76267	A0	22.9	17	0.19	...	1.74E+01	...	Pourbaix et al. 2004; Eggleton & Tokovinin 2008
HIP 81126 ^b	B9	92.7	157	10.2	...	5.56E+03	...	Sixth Catalog of Orbits of Visual Binary Stars
HIP 81641	A1	92.9	57	13.7	6477.0	9.12E+03	7.24E+07	Tokovinin 1997; Eggleton & Tokovinin 2008
HIP 90185	B9	44.3	155	105.9	...	2.13E+05	...	Eggleton & Tokovinin 2008
HIP 92024	A7	29.2	2	1927.2	...	2.30E+07	...	Eggleton & Tokovinin 2008

Table 2—Continued

Name	Spectral Type	Dist. (pc)	R_{dust} (AU)	S1 (AU)	S2 (AU)	P1 (days)	P2 (days)	References
HIP 92680	K0	49.7	11.3	19.9	...	2.74E+04	...	Billier et al. 2010
HIP 95261	A0	47.7	15	198.9	...	6.91E+05	...	Eggleton & Tokovinin 2008
HIP 99473	B9	88	213	0.28	...	1.71E+01	...	Shatskii 1998; Pourbaix 2000; Pourbaix et al. 2004; Eggleton & Tokovinin 2008
HIP 101800	A2	54.3	31	0.15	...	1.10E+01	...	Pourbaix et al. 2004; Eggleton & Tokovinin 2008
HIP 107649	G2	15.6	27	858.0	...	8.38E+06	...	Eggleton & Tokovinin 2008
HIP 113368	A3	7.7	73	54380	...	3.28E+09	...	Barrado y Navascues et al. 1997

Note. — List of multiples in our debris disk sample. Columns S1 and S2 denote the binary/multiple separation and likewise P1 and P2 denote the period of the orbit.

^a— While HIP 11437 is not explicitly labeled as a binary in the β Pic moving group (Zuckerman & Song 2004; Torres et al. 2008), the kinematics, distance, and close proximity of BD+30 397B suggest these two stars are a physically bound \sim 1000 AU binary system.

^b— Two periods are commonly listed for HIP 81126: $P = 15.2$ or 7.48 years ($a = 0.11$ or $0.074''$; Mason et al. 2001). While Eggleton & Tokovinin (2008) adopt the 7.48-year period, we chose to use the 15.2-year period as this is fit well in the Sixth Orbit Catalog of Visual Binary Stars with recent measurements (Brendley & Hartkopf 2007) and is the period adopted in other recent papers (Cvetkovic & Ninkovic 2010; Mason et al. 2009).

Table 3. Multiplicity Fractions

Spectral Type	Number	Percent	From ET08	From DM91
B	5/6	83_{-23}^{+6}
A	12/47	26_{-5}^{+7}	46.0	...
F	5/41	12_{-3}^{+7}	47.4	...
G	4/12	33_{-10}^{+15}	45.0	57
K	2/5	40_{-16}^{+21}	29.1	...

Note. — Fraction of multiple stars (all as percentages) broken down by spectral type of the primary star with comparisons from the literature (ET08: Eggleton & Tokovinin 2008; DM91: Duquennoy & Mayor 1991).

Table 4: IRCAL Debris Disk Observations

Name	UT Date	Filter	Exposure Time (s)
HIP 63076	2009 June 7	Ks	11.4
HIP 70952	2009 June 7	J,H,Ks	20, 11.4, 11.4
HIP 71284	2009 June 7	BrG-2.16	20
HIP 76635	2009 June 7	Ks	20
HIP 78554	2009 June 7	Ks	11.4
HIP 81800	2009 June 7	Ks	11.4
HIP 83480	2009 June 7	Ks	20
HIP 85157	2009 June 7	Ks	11.4
HIP 85537	2009 June 7	Ks	11.4
HIP 87108	2009 June 7	BrG-2.16	40
HIP 106741	2009 June 7	Ks	40
HIP 5626	2009 October 29	Ks	52
HIP 15197	2009 October 29	BrG-2.16	52
HIP 10670	2009 October 29	BrG-2.16	26
HIP 32480	2009 October 29	BrG-2.16	56
HIP 35550	2009 October 29	BrG-2.16	54
HIP 41152	2009 October 29	Ks	26
HIP 41307	2009 October 29	BrG-2.16	52
HIP 69732	2010 August 3	J,Fe II,BrG-2.16	6, 4.2, 3
HIP 1185	2010 August 4	Ks	20

Table 5. IRCAL Calibrations

Name	Grade	PA (deg)	ρ (")	ΔX (pixels)	ΔY (pixels)	Calc. PA (deg)	Calc. ρ (")
HD 212698	4	41.4	1.30	-11.76	11.98	43.1	1.26
HD 165341	1	130.8	5.77	-60.70	-47.76	130.6	5.76
GJ 65	3	43.1	1.96	-18.72	19.98	41.8	2.06
HD 38	4	186.6	5.94	7.73	-77.12	185.9	6.00
HD 38	4	186.2	6.04	7.73	-77.12	185.9	6.00
HD 133640	2	60.1	1.54	-18.40	9.89	60.7	1.54
HD 160269	3	315.7	0.99	9.32	8.73	315.5	0.96
HD 146361	4	237.5	7.12	81.90	-49.00	237.9	7.06

Note. — Stars used as part of our IRCAL calibration, as described in Section 4.1. Grade denotes the quality of the orbit, with lower numbers representing better orbits. The two columns after Grade denote the position angle (PA) and separation (ρ) for the system at the time of our observations. ΔX and ΔY are the pixel separation in the X and Y direction and the two columns following that are the calculated position angle and separation using the best-fit solution in Section 4.1.

Table 6: Unstable debris disk systems

Name	Sep. (AU)	R_{dust} (AU)	Ratio	Type	Stability (%)
HD 1051	628	173	0.28	binary	6
HIP 35550	126	71	0.57	triple	1
HIP 42430	34	21	0.62	binary	1
HIP 76127	66	171	2.58	binary	0.1
HIP 90185	106	155	1.46	binary	0.2
HIP 92680	20	11	0.57	binary	1
HD 46273	26	16	0.62	quintuple	1
HD 80671	3.4	2.9	0.87	triple	0.6
HD 127726	14	28	1.96	triple	0.1

List of unstable systems with the ratio of the dust to star separation. For completeness, we include the 3 systems from Trilling et al. (2007) at the bottom of the list. The final column denotes the probability that the inclination and location of the secondary star along a circular orbit are such that in actuality the system lies outside of the unstable zone (see Section 6 for details).

Table 7. Resolved Debris Disks

Name	R_{res} (AU)	λ (μm)	Type	T_{dust} (K)	R_{BB} (AU)	Refs
HD 139664	83	0.6	scattered	80, 50	21, 61	Kalas et al. 2006; Chen et al. 2009
HD 15115	430	0.61	scattered	65	35	Kalas et al. 2007a; Rhee et al. 2007
HD 61005	210	1.1	scattered	58	17	Hines et al. 2007; Hillenbrand et al. 2008
HD 53143	82	0.6	scattered	80	9	Kalas et al. 2006; Rhee et al. 2007
AU Mic	130	0.6	scattered	50	9	Kalas et al. 2004; Rhee et al. 2007
HD 207129	163	0.6	scattered	55	27	Krist et al. 2010; Rhee et al. 2007
HD 181327	86	1.1	scattered	75	25	Schneider et al. 2006; Rhee et al. 2007
HD 15745	300	0.59	scattered	85	22	Kalas et al. 2007b; Rhee et al. 2007
HR 4796A	70	1.1	scattered	110	30	Schneider et al. 1999; Rhee et al. 2007
Fomalhaut	141	0.6	scattered	65	73	Kalas et al. 2005; Rhee et al. 2007
HD 141569A	185	1.1	scattered	110	24	Weinberger et al. 1999; Rhee et al. 2007
HD 92945	54	0.6	scattered	45	23	Golimowski et al. 2011; Rhee et al. 2007
Vega	85	70, 160	thermal	80	93	Sibthorpe et al. 2010; Rhee et al. 2007
HD 107146	97	1300	thermal	55	29	Corder et al. 2009; Rhee et al. 2007
HD 32297	115	12–19	thermal	85	28	Moerchen et al. 2007; Rhee et al. 2007
HD 10647	85	70	thermal	65	22	Liseau et al. 2010; Rhee et al. 2007
HR 8799	200	70	thermal	150, 45	9, 95	Su et al. 2009
HD 191089	59	18.2	thermal	95	15	Churcher et al. 2011; Rhee et al. 2007
η Tel	24	18.3	thermal	150	15	Smith et al. 2009; Rhee et al. 2007
ϵ Eri	60	850	thermal	40	27	Greaves et al. 1998; Rhee et al. 2007
η Crv	145	100	thermal	354, 31	174, 1.4	Matthews et al. 2010
β UMa	47	100	thermal	109	51	Matthews et al. 2010
β Leo	39	100	thermal	112	23	Matthews et al. 2010
HD 98800B	13	880	thermal	160	2.2	Andrews et al. 2010; Low et al. 2005

Note. — Disk radii (R_{res}) for resolved systems. This table is not meant to represent the most descriptive values for the system (for example, some disks are clearly asymmetric); we refer the reader to the individual references for details. For systems resolved in both thermal and scattered emission, we list only the thermally resolved radius. Resolved and blackbody-fit radii are compared in Figure 9.

Table 8: Debris disk dust masses

Name	λ_{dust} (μm)	F_{ν} (mJy)	Mass (M_{moon})	Age (Myr)
AU Mic	850	14.4 ± 1.8	0.5	12
β Pic	1300	24.9 ± 2.6	5.8	12
HIP 95270	870	51.7 ± 6.2	36.5	12
HIP 99273	350	54 ± 15	2.2	30
HIP 114189	850	10.3 ± 1.8	6.3	30
HIP 16449	870	17.6 ± 8	33.1	50
HIP 10670	850	5.5 ± 1.8	1.8	100
HIP 36948	350	95 ± 12	2.5	100
HIP 11360	850	4.9 ± 1.6	2.9	100
HIP 60074	850	20 ± 4	5.7	100
HIP 22226	870	6.9 ± 5	13.4	100
HIP 87108	870	12.8 ± 5.2	2.6	200
HIP 101612	870	13 ± 7.1	3.2	200
HIP 6878	1200	3.2 ± 0.9	4.5	200
HIP 90936	870	18 ± 5.4	9.7	200
Vega	1300	11.4 ± 1.7	0.6	220
η Crv	850	7.5 ± 1.2	0.3	300
HIP 32480	850	5.5 ± 1.1	0.5	600
ϵ Eri	1300	24.2 ± 3.4	0.4	730
σ Boo	850	6.2 ± 1.7	0.7	1000
Fomalhaut	850	97 ± 5	1.7	220
HIP 107649	870	5.1 ± 2.7	0.5	600
HIP 27072	850	2.4 ± 1	0.04	1000

Disk dust masses for Table 1 stars listed in Nilsson et al. (2010). The last three systems are binaries. λ_{dust} is the wavelength at which the dust is detected and the one used to estimate dust mass (see Section 7); dust temperatures and distances from Earth are listed Table 1.

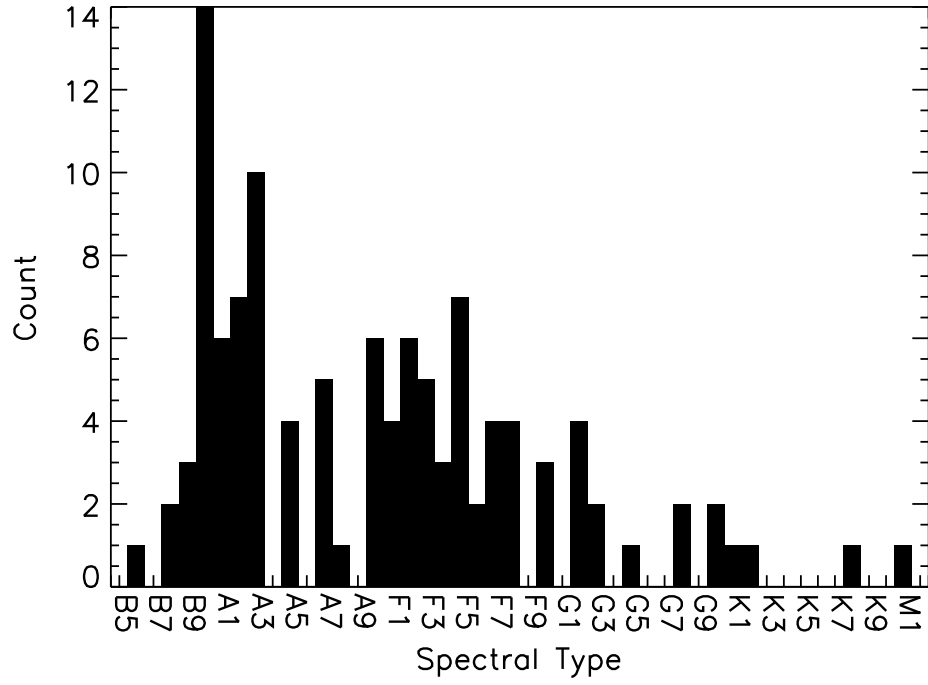


Fig. 1.— Spectral type distribution of our 112-star debris disk sample.

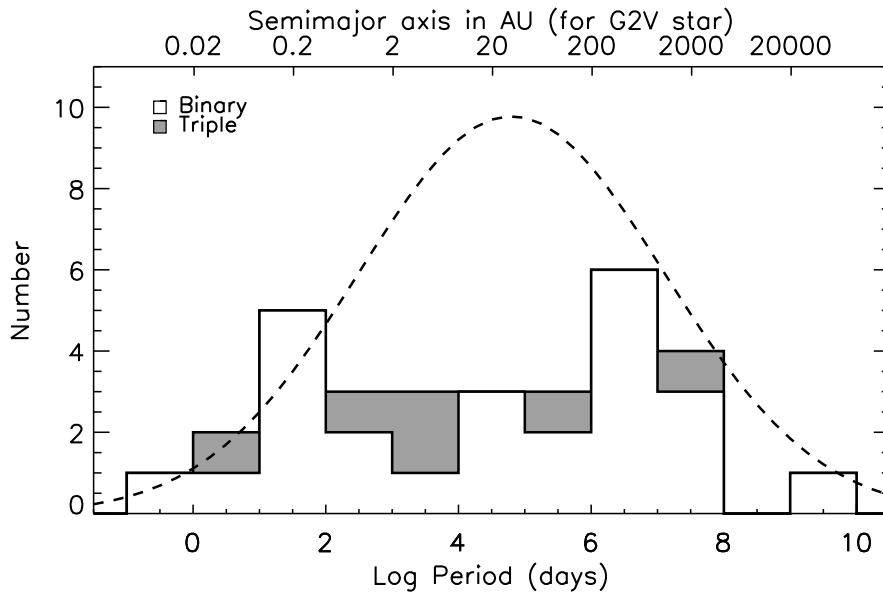


Fig. 2.— Period distribution of our debris disk sample. For triple systems, we include both periods (for example, the A-B period and the AB-C period). For comparison, the semi-major axis for a sun-like star is displayed on top. The dashed line illustrates the expected period distribution from Duquennoy & Mayor (1991) (and very similar to Eggleton & Tokovinin 2008) normalized to contain the expected number of binaries or multiples in the sample ($112 \times 0.5 = 56$ multiples). While the short and long period binary distribution approximately matches the Duquennoy & Mayor (1991) distribution, there is a lack of systems with intermediate periods (separations $\sim 1 - 100$ AU).

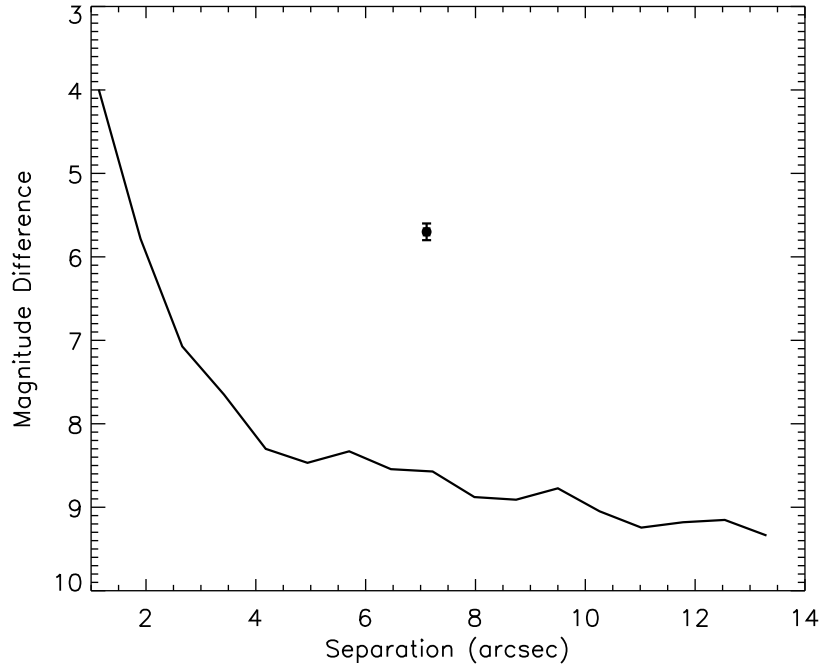


Fig. 3.— Magnitude limits (5σ) in the Ks filter as a function of separation for our HD 1051 (HIP 1185) data. Limits are obtained by performing 2-pixel radius aperture photometry (the same as for HD 1051B) at random locations in annuli around the primary. The standard deviation of these measurements provides an estimate of the noise. The detected companion is plotted as a circle.

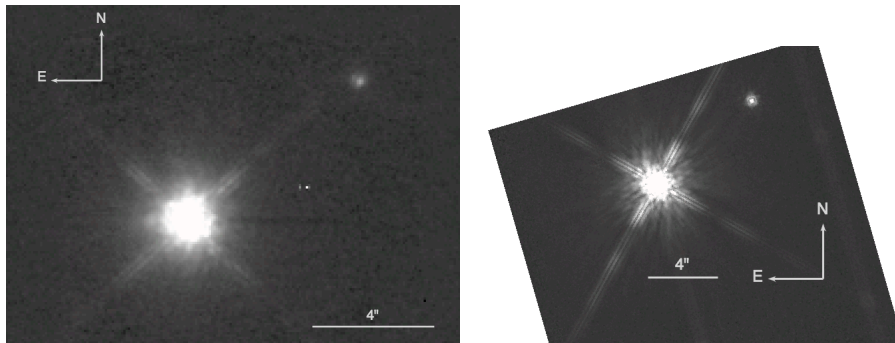


Fig. 4.— Lick IRCAL (left) and HST NICMOS image (right) for HD 1051.

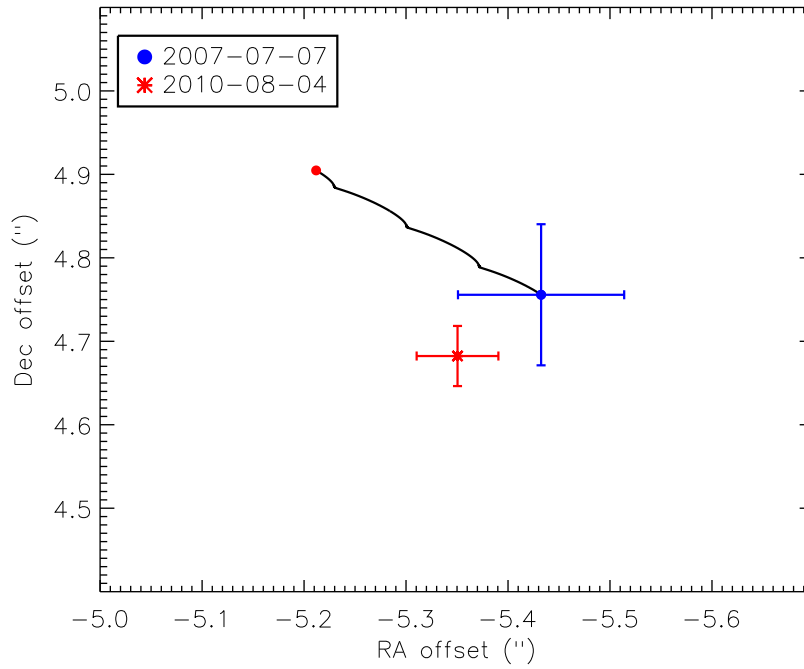


Fig. 5.— Measured offsets for HD 1051B in Lick IRCAL and HST NICMOS data. The black line illustrates the motion relative to HD 1051 of a stationary background object over the 3-year period. The circle at the end of the black line is the predicted location of a background object in 2010.

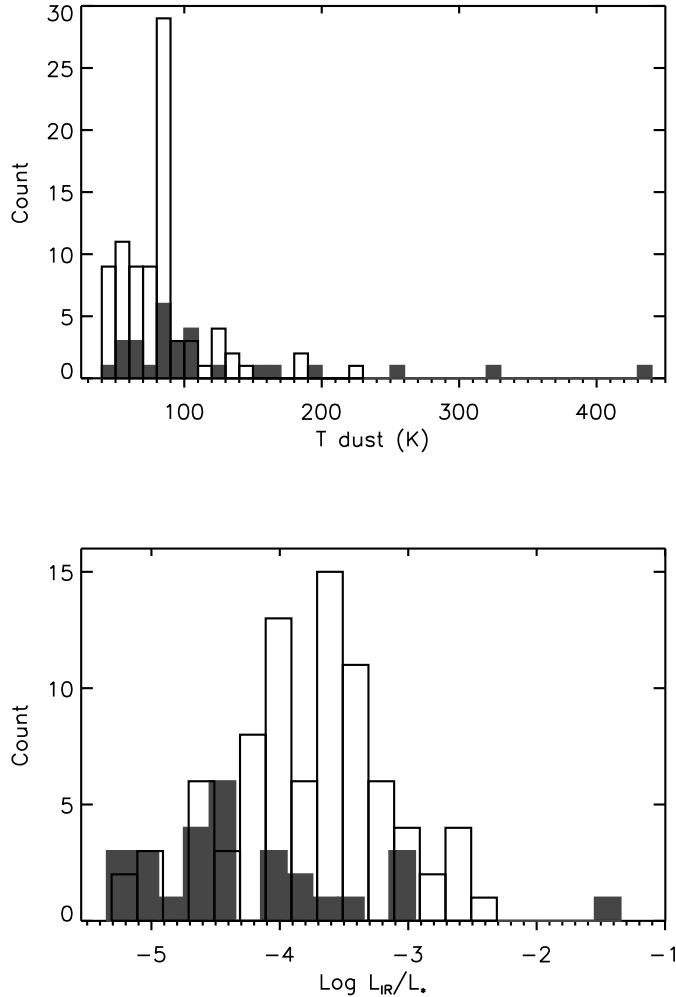


Fig. 6.— Dust temperatures (top) and fractional luminosities (bottom) for our debris disk sample. Open bars represent single systems, while the shaded bars represent multiples. The large number of systems in the $\sim 70 - 90$ K bin is partially an artifact of the analysis and includes systems with detections at only 60 or $70\mu\text{m}$, see discussion in Section 5. While the dust temperatures are similar for both single and multiple systems, the fractional luminosities for single stars are, on average, 2–3 times larger than those for multiple stars. BD +20 307 is the rightmost system in both panels (Weinberger et al. 2011).

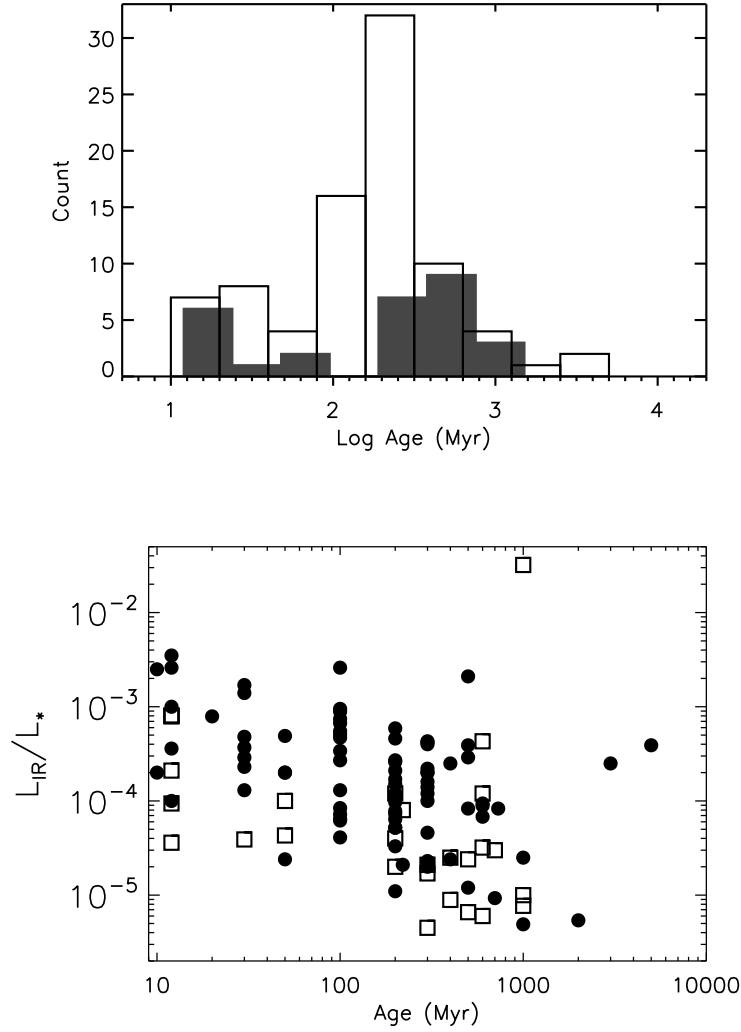


Fig. 7.— Age distribution in our debris disk sample. Open bars represent single systems, while the shaded bars represent multiples. While the histogram (top) suggests more multiple systems are older compared to the single stars, the plot of fractional luminosity vs. age (bottom; circles are single stars, squares are multiple systems) shows that at any given age, multiple stars are more likely to have lower fractional luminosities compared to single stars. The ~ 1 Gyr-old binary system with $L_{\text{IR}}/L_* \sim 0.03$ is BD +20 307.

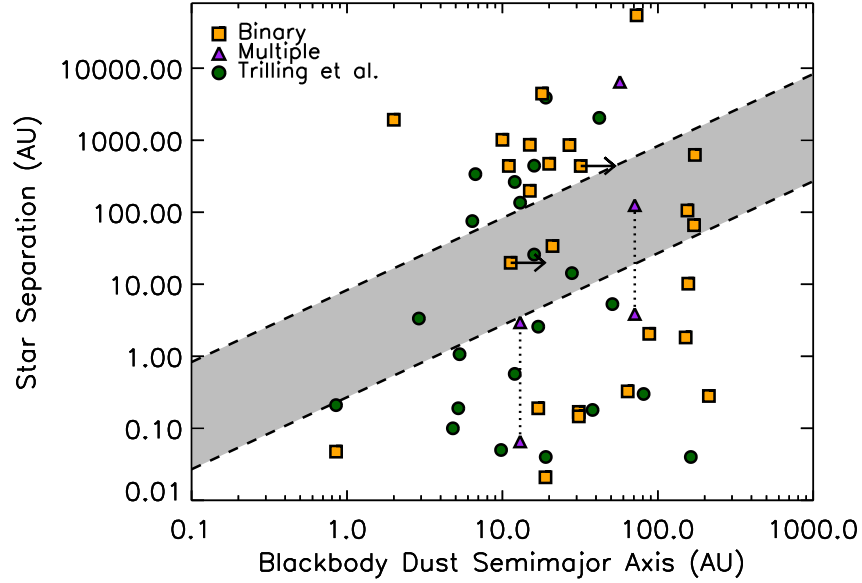


Fig. 8.— Stellar separation versus blackbody dust semi-major axis for debris disk stars including those from Trilling et al. (2007). Triple systems are plotted at both orbital separations with a dotted line connecting them; the exception is HIP 81641 where the disk may be around the single primary so the separation of the companion close binary is not relevant. The two systems with right pointing arrows are HIP 66704 and HIP 92680 (PZ Tel), for which dust emission is detected only at $70\mu\text{m}$; for clarity we do not label the systems with excesses detected only at $60\mu\text{m}$ (see Section 5). The grey region in the plot highlights where the gravitational field of a companion is expected to significantly affect dust in the system (see the first paragraph of Section 6)

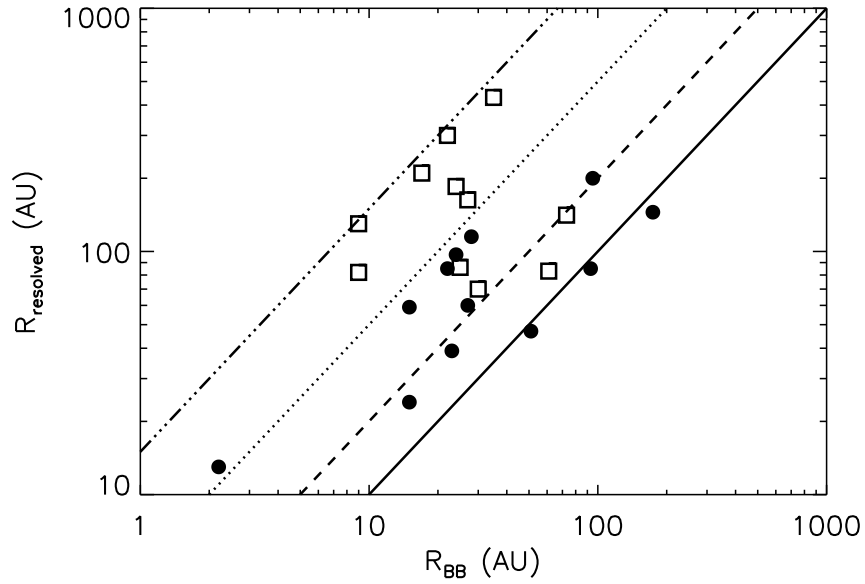


Fig. 9.— Resolved vs black body disk radii for debris disks as listed in Table 7. The lines represent ratios of 1:1 (solid), 2:1 (dashed), 5:1 (dotted), and 15:1 (triple-dot-dashed) when comparing resolved disk sizes to those inferred from blackbody fits. Circles are disks resolved in thermal emission, while squares are disks resolved in scattered light. Thermally resolved disks have sizes $\sim 1 - 5$ times that estimated from the blackbody SED, whereas disks resolved in scattered light tend to be more extended.